

Systematic Generation of Arbitrary Antenna Geometries

Ekrem Altinozen, *Student Member, IEEE*, Ian Harrison, Ana Vukovic, *Member, IEEE*, Phillip Sewell

Abstract—Applications for conformal, wearable antennas are growing for consumer electronics. Hence, it is important to assess to what degree antenna performance can be tolerant to in-situ deformations that can take the form of bending, crumpling and twisting and combinations of these effects. However, generating geometries of arbitrary antenna deformations such as bending, crumpling and twisting, that can be processed by standard electromagnetic software is a major challenge that significantly complicates full assessment of in-situ antenna performance. Constructive Solid Geometry methods of generating geometries is difficult to robustly apply to non-conformal antennas and more flexible techniques required to progress the antenna studies further. To address this challenge, this paper investigates the utility of the Green Coordinate method for spatial manipulation of 3D objects. First a calibration of a straightforward application of the GC method against a reference case of a patch antenna bent over a cylindrical surface, which can also be generated exactly, is undertaken. The paper shows that systemic scaling distortions are introduced by the GC method and introduces a compensation method that can overcome these distortions. Subsequently, the compensated method is used to obtain new predictions of the electromagnetic performance of patch antennas with deformations.

Index Terms— computational electromagnetics, conformal antenna, microstrip patch antenna, antenna deformations, space deformation technique, Green Coordinates

I. INTRODUCTION

Wearable and foldable electronics can receive, store or transmit digital information and are the focus of increased attention in many areas including healthcare, entertainment and the sports industry. Individual components such as RFIDs, medical sensors and antennas can be integrated into a variety of substrates including knits, embroidery or non-woven materials [1-3]. More generally, non-flat antennas are routinely found mounted on curved surfaces such as airplane wings and fuselages [4] and as 5G antenna arrays on cylindrical surfaces [5]. The design and integration of individual antennas is often a crucial aspect in the overall system design.

One of the most challenging cases for predicting in-situ performance is that of wearable textile antennas fabricated on woven and non-woven materials that will experience bending, twisting and crumpling when pulled in different directions by

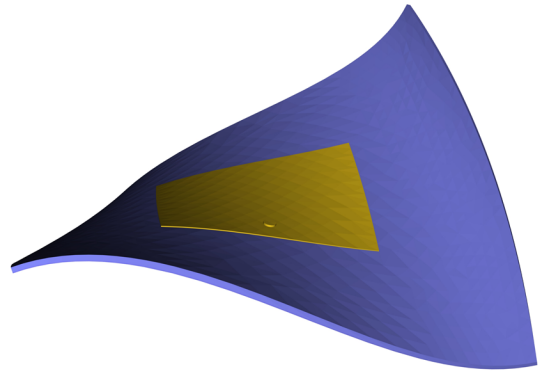


Fig. 1. Arbitrary patch antenna deformation with crumpling along the width of antenna and twisting along the length of antenna

human activity, as illustrated in Fig. 1. Whilst woven and non-woven materials are more stable than knits, [1], it is still expected that all textile antennas will to some extent, experience elongation and compression when in use.

To date there has been an increasing effort to predict performance changes caused by antenna deformations but these have primarily focused on patch antennas and antenna arrays [6-16] bent over *cylindrical surfaces*. The results reported were mainly obtained from practical measurements [6, 7] and only a few predictive results have been reported using the modelling techniques embodied in CST's and Ansys software [8, 9, 14, 15]. Both the experimental and simulated results demonstrate that bending has a significant influence on antenna performance; specifically, increased curvature decreases the overall gain of antenna and shifts the resonant frequency, although the bandwidth does remain approximately the same across all measured cases [6, 8, 9, 11, 14-16].

The virtually exclusive focus of previous work on purely cylindrical deformations can be attributed to the difficulty in robustly generating *arbitrary deformed antenna geometries* suitable for predictive simulations. Clearly, to advance understanding and to develop practical design guidelines, the problems associated with generating arbitrary geometries need to be fully understood and resolved and this motivates the contribution presented in this paper.

This paragraph of the first footnote will contain the date on which you submitted your paper for review.

This work was supported in part by Turkey Education Embassy Scholarship Programme.

The authors are with the George Green Institute for Electromagnetics research, School of Electrical and Electronic Engineering, The University of Nottingham, Nottingham University Park, NG7 2RD, Nottingham, UK. (e-mail: ekrem.altinozen1@nottingham.ac.uk; ezaih2@exmail.nottingham.ac.uk; ana.vukovic@nottingham.ac.uk; phillip.sewell@nottingham.ac.uk;)

The specific and critical CAD issue for the generation of deformed antenna geometries is to obtain well behaved and consistent interfaces between the different elements that make up the antenna. This is clearly illustrated by a finite thickness metal patch on a substrate: Either the patch and the substrate are generated separately as deformed parts and *stitched* together or, a flat patch-substrate combination is generated with a well behaved interface, which is easy to do, and this combination is deformed to the final desired geometry. This paper discusses the superiority of the latter approach and then demonstrates its practical implementation in a straightforward manner.

It is important to explain the phrase *a well behaved interface*. Stitching together non-coordinate aligned and separately created parts inevitably leads to *dirty interfaces* that do not perfectly align and typically have microscopic non-physical *gaps* and *overlaps* which are disastrous for subsequent mesh generation and electromagnetic (EM) simulations. At best, *dirty interfaces* result in unrealistically small mesh cells that severely compromise the computational efficiency and at worst, mesh generation proves impossible. It is commented here that the subsequent choice of modelling method, Finite Elements, Finite Differences, Method of Moments, or their implementation within particular software packages is not the issue, rather it is the geometrical data upon which they operate that has the failing.

Experience shows that even the CAD models generated using mechanical software need *CAD repair* techniques to clean these interfaces lacks robustness and require significant manual intervention.

Overall, the number of trial cases a designer can easily consider is severely curtailed which explains the existing focus on purely cylindrical geometries that are amenable to exact generation [8-11, 15, 17]. To avoid the issue of dirty interfaces, the strategy pursued here is to generate flat antenna geometries and deform them holistically using a technique borrowed from computer graphics.

Computer graphics offers a number of techniques for spatial manipulation of 3D objects, for example Mean Value Coordinates (MVC), Harmonic Coordinates (HC) and Green Coordinates (GC) [18-21]. The common feature of these techniques is to enclose the object of interest by a so called bounding *cage* that has a similar, but less complicated shape than the object of interest. All spatial points within the interior of the cage can be expressed in terms of the cage's geometry (e.g. vertex locations in the case of MVC) and by subsequently manipulating the simple cage, for example interactively *dragging* one of its vertices, smooth deformations are induced into the complex geometry of the enclosed object. The appeal of fast and simple modification of characters for animations is exactly the feature that is also sought here for systemic performance studies on deformed antennas.

Each of the particular methods listed above differ in (i) the extent to which they preserve the *physically realistic* nature of practical deformations of the object's shape (shape-preserving property) and (ii) the efficiency of their numerical implementation, i.e., either exploiting closed form formulae or

requiring substantive numerical processes [20]. Shape preservation in the context of this work is a measure of whether the object deformation follows the expected behavior of stress-strain physics which is clearly desirable. Two points to note here are that (i) it would be difficult to theoretically express the complexity of such deformations in the general case with a view to explicitly *code* geometry generation, vertex by vertex, as one can obviously do for the purely cylindrical case, and (ii) the scope of this work does not extend to the further complexities of the materials, for example the opening and closing of woven fabrics.

The Green Coordinates approach, described in more detail below, stands out from the alternatives listed above as that which best preserves the shape of 3D objects and is implemented using only closed form analytical formulae [20, 21]. The good shape preservation properties trace to the fact that the two-dimensional (2D) and three-dimensional (3D) GC method induce purely conformal and quasi-conformal maps respectively with minimal anisotropic scaling [20, 21].

Earlier work has demonstrated the use of the GC method to generate arbitrarily deformed antenna geometries [22, 23]. However, whilst successful, the approach does introduce systemic global distortion of the resulting antenna geometry and removing this is a first objective here. For clarity, we use the term *deformation* for the desired change of shape of an antenna from the flat to the in-situ case and *distortion* to denote these undesirable systemic errors.

A suitable benchmark geometry for assessing and then removing the GC distortions is the purely cylindrical case as it is a developable surface that ought to be generatable without any distortion. This work strongly emphasizes the quantification of antenna deformations in the context of the subsequent impact on performance, characterized by reflection coefficient S_{11} and radiation pattern, and therefore, the next few paragraphs will describe the meshing and simulation approaches providing this context.

As the antennas under investigation are clearly not coordinate aligned, discretization with an unstructured mesh is advantageous for minimizing discretization errors and managing computational effort. An in-house 3D Delaunay Mesher and unstructured mesh EM Transmission Line Modelling (TLM) simulator have been used [24-26].

The Delaunay mesher [26] is a robust 3D implementation of the techniques described in [27] augmented by many features that ensure that the meshes produced are sympathetic to the needs of subsequent large-scale EM simulation and has been widely used for the purpose [28-34].

The unstructured TLM method is a well established extension to the Cartesian mesh TLM method, the latter having over 50 years of practical use for EM simulations [35, 36]. The TLM approach has the distinct advantages that all field component samples are co-located in time and space, and crucially, that stability is provable on a cell-by-cell basis without resorting to estimators such as the Courant condition. For large-scale simulations this is a critical advantage and late time instability has never been observed with TLM. The unstructured mesh variant of the TLM algorithm has been

demonstrated to be second order accurate with respect to wavelength, provide both smooth boundary and graded mesh capabilities, and has been industrially characterized and deployed for a range of applications including EMC and aerospace [29, 31, 37] and readers are specifically referred to [24, 25] for further details.

The remainder of this paper is structured as follows: Section II provides an overview of the Green Coordinates method; Section III investigates the impact of the GC parameters on antenna distortions and Section IV introduces a simple GC compensation method. The effectiveness of this is assessed by comparing the EM performance of compensated-GC antennas with the special case of cylindrical bending whose geometries are in closed form. Finally, Section VI demonstrates the performance of antennas bent over double curved surfaces compared to the flat case, which are new results beyond the possibility of using CSG (Constructive Solid Geometry), to straightforwardly generate the geometries. Section VII gives the overall conclusions of the paper.

II. GC METHOD FOR GENERATING CYLINDRICALLY BENT ANTENNAS

Green Coordinates are a method for spatial manipulation of objects that belongs to the class of methods where a cage of a simple polyhedral shape encloses the object of interest [20, 21]. In the case of a flat microstrip antenna the undeformed cage is a segmented cuboid and the antenna is positioned in the middle of it surrounded by a padding of length Δ , as shown in Fig. 2a). Here, the same padding is used in all directions. The theoretical basis of the GC method is that the spatial coordinate variable \mathbf{r} within the cage satisfies Laplace's equation and thus introduction of a Green's function and use of Green's third identity expresses the value of any particular point \mathbf{r}_p within the cage as an integral of the values of \mathbf{r} and its normal derivative over the cage surface. For a triangulated cage surface, these integrals can be evaluated in closed form such that \mathbf{r}_p is expressed as a discrete and finite extent superposition of the cage's vertices, \mathbf{r}_v , and face normals, \mathbf{n}_f , total number of vertices, N_v , and faces, N_f , with suitable coefficients g_v^V and g_f^F [20, 21],

$$\mathbf{r}_p = \sum_{v=0}^{v=N_v} \mathbf{r}_v g_v^V(\mathbf{r}_p) + \sum_{f=0}^{f=N_f} \mathbf{n}_f g_f^F(\mathbf{r}_p) \quad (1)$$

The key point to note is that the *continuous* space within the cage (or in practice here, the relatively large number of topologically related vertices defining the object being deformed) is expressed in terms of a relatively few discrete quantities. The GC method deforms the enclosed space by making a one-to-one mapping of the set $\mathbf{r}_v \rightarrow \mathbf{r}'_v$ (and consequently $\mathbf{n}_f \rightarrow \mathbf{n}'_f$) and using the above superposition with the same weight coefficients as before, i.e.

$$\mathbf{r}'_p = \sum_{v=0}^{v=N_v} \mathbf{r}'_v g_v^V(\mathbf{r}_p) + \sum_{f=0}^{f=N_f} \mathbf{n}'_f g_f^F(\mathbf{r}_p) \quad (2)$$

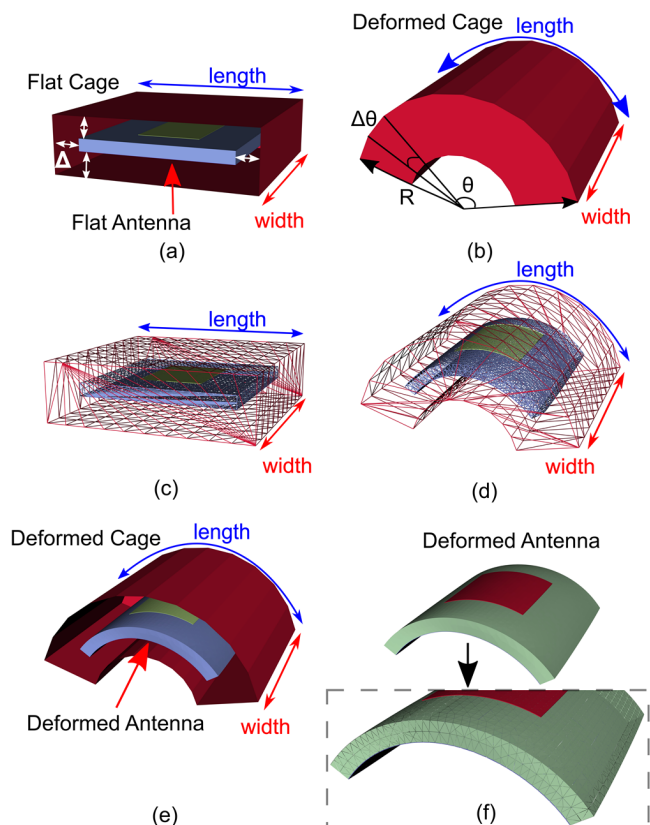


Fig. 2. a) Microstrip antenna placed inside the flat cage separated by a padding Δ from the edges of the cage; b) deformed cage for the case of cylindrical bending; c) same as a) but showing vertices and faces; d) same as b) but showing vertices and faces; e) deformations of the warped cage are transferred onto the antenna and f) deformed cage is removed to reveal the final result of deformed antenna and, in the inset, its surface triangulation.

By definition the flat cage is chosen to be a simple shape capturing only the global spatial characteristics of the enclosed object so that it is easy for a user to manipulate its overall shape by relocating (dragging and dropping) a few of its defining vertices to yield a *deformed cage*, (Fig. 2b). This is to be compared with attempting to manually deform the antenna, vertex by vertex, in a topologically consistent and physically realistic manner, which is clearly untenable in general. The full detail of the GC method is not given here and the reader is referred to the available literature on the method and the particular closed form expressions used [20, 21].

The GC methodology is implemented in our in-house Geometry Kernel (GK) [26] which also contains an extension to the published GC approach in order to avoid self-intersection of the deformed object. As the GC method does not embody an affine transformation, deforming long straight edges defined by a pair of end points, for example the sides of the patch, cannot be achieved by simply deforming the end vertices. An iterative splitting of such edges is required which terminates when the deformed midpoint of the edge coincides, within a given tolerance, with the linear interpolation of the deformed end points. For reference, we will refer to this tolerance as the *edge split tolerance* and all the results presented below used a value of 0.01 mm.

III. ASSESSMENT OF GC INDUCED DISTORTIONS FOR THE CASE OF CYLINDRICALLY BENT ANTENNA

In this section the distortions from the target deformation introduced by the GC method are quantified. The degrees of freedom examined are first the complexity of the cage used. This is quantified by the number of piece-wise segments used to describe the undeformed cuboidal cage, each of which deforms to one of the piecewise sectors of angle $\Delta\theta$ seen in the deformed cage of Fig. 2b) and more dramatically in Fig. 3a,b) below. The second degree of freedom is the extent of the padding, Δ , shown in Fig. 2a).

The figure of merit used to assess the undesirable distortion of the geometry is chosen to be consistent with one of the simple parameters used to design standard patch antennas, the radiating surface area. In fact, both the total (top + bottom + sides) surface area of the radiating patch and the total surface area of the substrate are observed noting that the intention is to deform a flat antenna of prescribed patch area into curved antenna with the same patch area (which is only exactly possible for developable surfaces). The relative distortion surface error, ρ , is thus defined as $\rho = (A_{GC} - A_{Flat})/A_{Flat}$, where A indicates the surface area of either the metallic patch or the substrate.

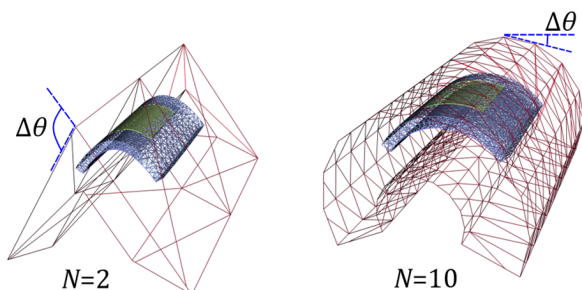


Fig. 3. The antenna geometry generated with $N = 2$, $N = 10$ segments in the cage definition.

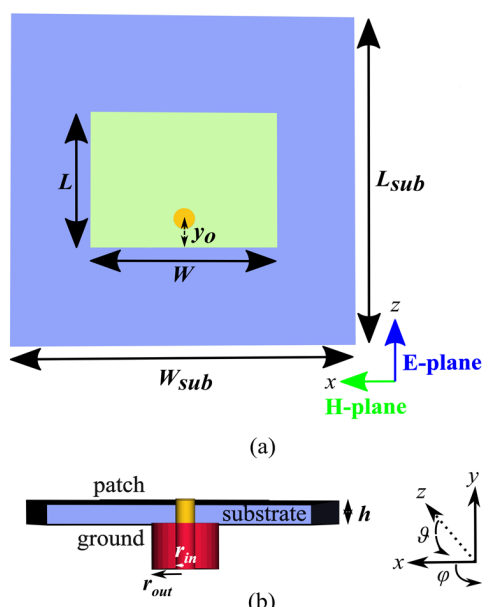


Fig. 4. The schematic of the flat patch antenna a) top view and b) side view. The angles ϑ and φ define E and H plane of the antenna radiation pattern, respectively.

The microstrip patch antenna used for this study is designed to resonate at 10.4 GHz and has patch width, W , of 10.830 mm and length, L , of 8.177 mm as shown in Fig. 4a,b). The substrate is Rogers Corporation Duroid 5880 of relative permittivity 2.2, width, W_{sub} and length, L_{sub} , of 20 mm and thickness, h , 1.575 mm. The antenna is fed from below by a coaxial cable positioned at $(W/2, y_0)$ where $y_0 = 1.75$ mm. The coaxial cable has inner radius, r_{in} , of 0.625 mm, outer radius, r_{out} , of 2.16 mm, and the relative permittivity of the sheath is 2.2. The metallic patch and the ground plane of the antenna both have a thickness of 0.035 mm and are treated as perfect conductors. The radius of curvature in the results below is defined to the bottom plane of the patch.

There are two potential causes of undesirable distortion; poor choice of method parameters and any systematic spatial stretching introduced by the GC method. This section seeks to identify the latter by converging to eliminate the former.

The relevant GC method parameters are the padding, Δ , and the number of piece-wise segments, N , that are used to describe the cross section of the cage as illustrated for $N=2$ and $N=10$ in Fig. 3.

An understanding of the likely impact of these parameters may be gauged from the description of the space within the cage by the GC method in terms of solutions to Laplace's equation and that these solutions exhibit the usual smoothing behavior with distance from sharp features such as corners. Therefore, although the cage is actually polygonal, at sufficient distance from its boundaries, the Laplacian solutions will be more dominated by the large scale arc geometry that the cage approximates, rather than the exact detail of its piecewise linear nature. This behavior is clear in Fig. 3 for the case of $N=2$.

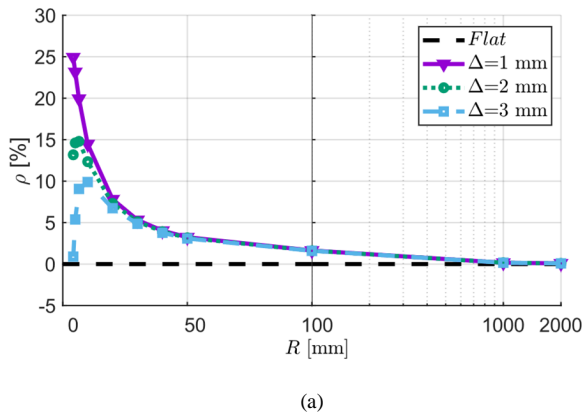
It is also noted that both using more segments in the cage, N , to approximate a fixed length antenna of given bending radius or increasing the bending radius for fixed N reduces the angular steps in the cage's boundary, $\Delta\theta$ in Fig. 3, that further smoothens the deformed space around the antenna.

It is tempting to conclude that one should use a large value of padding as this has no impact on the computational effort of the approach and ought to reduce the error. However, in the more general case, this would also mean loss of control of the detail of the antenna's deformation, so in fact there is a conflicting driver to minimize the padding. Similarly, although using a larger value for N would appear advisable, this does linearly impact on the computational cost.

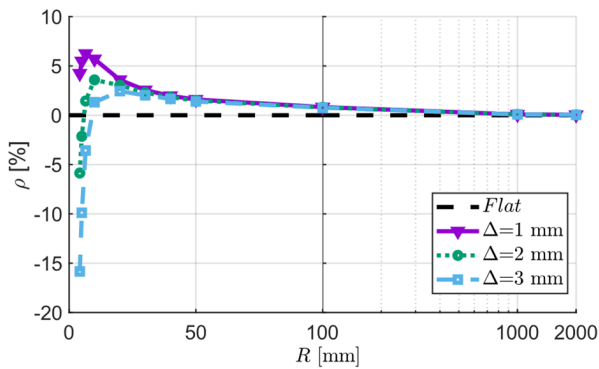
Figs. 5a,b) show the impact of the padding, Δ , on the relative surface distortion error, ρ , for both the metal patch and the substrate of the antenna, as the radius of curvature is varied with $N=10$ piece-wise segments used to describe the cross section of the cage. Similarly, Figs. 6a,b) fix the padding to $\Delta=3$ mm and vary N between 2 and 12 segments.

Together, these figures reveal that for bending radii above 50 mm the choice of Δ and N have negligible impact, but there remains a systematic error introduced by the GC method. For smaller radii, the errors do increase reaching a peak in some cases before rapidly increasing again with the opposite sign, i.e. the areas shrink rather than expand. In this regime, the choice of a larger Δ is appropriate, however there remains a remarkable insensitivity to the choice of N .

Overall it is noted that, given an antenna length of 20 mm,



(a)



(b)

Fig. 5. Relative surface distortions error of (a) metal patch and (b) substrate as a function of bending radius R and the padding Δ .

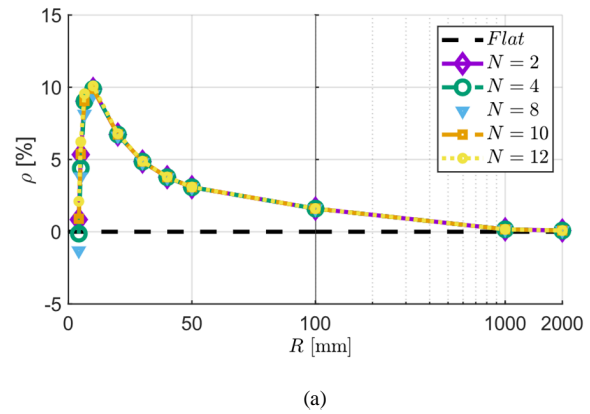
bending radii below 50 mm, are certainly severe deformations in shape, the systematic errors of Fig. 5 and Fig. 6 for all radii are deemed to be unacceptably large.

In fact, this is partially a positive result as the intention is to keep the cage as simple as possible. The explanation of the systematic error is actually found in a subtlety of the GC algorithm which is used to ensure that in the 3D case least deforming and quasi-conformal spatial deformations are produced [20, 21] compared to other space manipulation techniques. A local stretch factor appears in the 3D algorithm which although generally successful in preserving shape, does not decouple to the known 2D stretch factor and an axial stretch factor if the geometry happens to be separable as is the case for a cylinder.

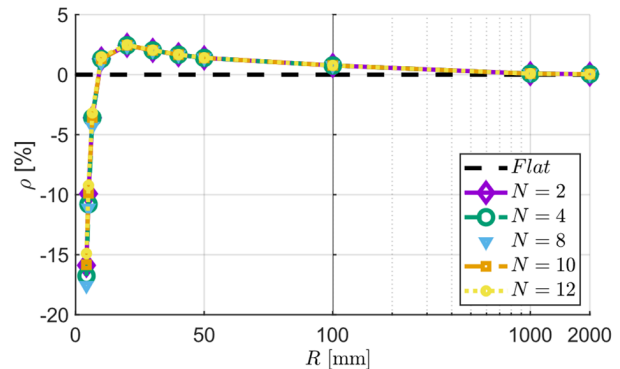
Therefore, it has been shown that GC method can simply produce bent antennas, but that a spatially varying stretch factor in its algorithm introduces an error that must be managed. In the context of textile antennas, the next section describes how this systemic error can be successfully compensated for on average.

IV. METHODS FOR COMPENSATING GC INDUCED DISTORTIONS

From an engineering viewpoint, the resonant frequency and radiation pattern are key performance metrics of an antenna and these are, for the above case of patch antenna, predominantly determined by the size of the radiating patch. Since the GC method does preserve the overall shape, pre-scaling of the size



(a)



(b)

Fig. 6. Relative surface distortion error of (a) metal patch and (b) substrate as a function of bending radius R and the number of cage segments N .

of the patch ought to minimize the distortions just observed. This section describes a straightforward pre-scaling method referred to as the *Width and Length (WL) compensation method*.

The compensation method is based on comparing the widths and lengths of the radiating patch before and after deformation. The width and length of the deformed patch are extracted by fitting a (x, y) order polynomial function, where x and y indicate the order of the polynomial function used along the width and length of the patch respectively. The actual width and length of the deformed patch are then analytically evaluated by integrating over the polynomial approximation.

Each of the ratios of the width and length of the radiating patch before and after deformation gives a scaling factor e.g. $s_W = W'/W$ and $s_L = L'/L$, with which the flat antenna can be scaled before the GC method is applied, i.e. $W \rightarrow W'/s_W$ and $L \rightarrow L'/s_L$.

This process is iterated until a prescribed relative difference in the width and/or length of the patch is satisfied and typically this converges within 3-5 iterations.

Fig. 7 compares the relative surface distortion error of the radiating patch with and without the pre-scaling compensation for a range of bending radii from 4.2 mm to 60 mm, the padding, $\Delta = 1$ mm and $N=10$ (i.e. as in Fig. 2a). It is clear that this relatively simple pre-scaling approach is highly effective at removing the undesirable patch distortion over a wide range of radii.

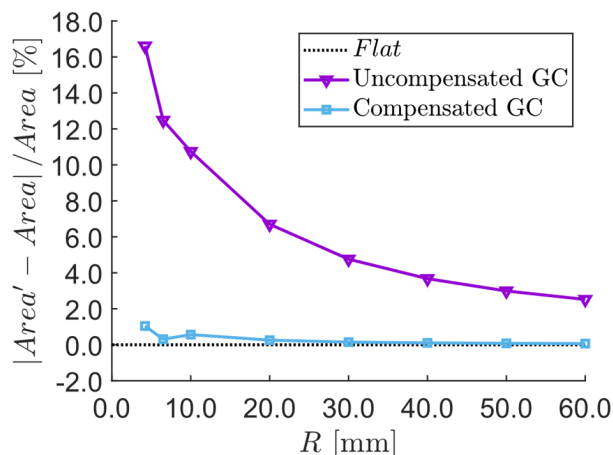


Fig. 7. Relative surface distortion error of GC generated antenna to that of the flat antenna for uncompensated GC method and compensated GC method.

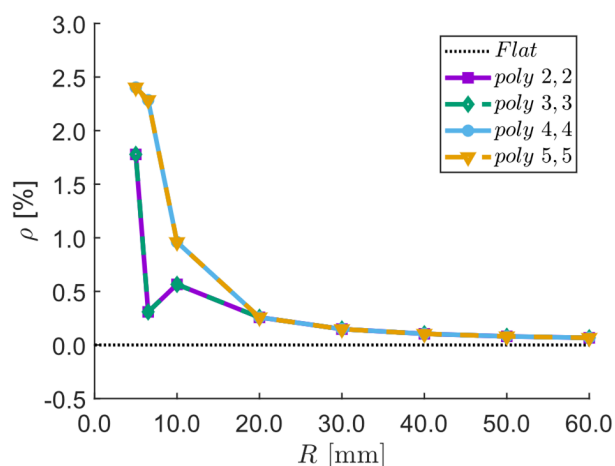


Fig. 8. Relative area error of WL approach for different degree of polynomials. The notation (*poly x, y*) indicates the order of the polynomial function used along the width and length of the patch.

It is important to adopt a good surface fitting approach for the GC compensation without incurring a notable computational cost. Fig. 8, confirms that the adequacy of a (3,3) order polynomial surface approximation. Slight improvement is obtained for higher order models for small radii (noting that symmetry pairs the curves), with virtually no impact on the approximately 3 mins calculation time of the overall deformation calculation.

Fig. 9 further explores how the area distortions decompose into width and length distortions and confirms that, as the bending is applied along the width of antenna, the largest distortion is occurring along the width of the patch.

V. EM PERFORMANCE OF CYLINDRICALLY BENT ANTENNAS

The previous results demonstrate the success of a simple distortion compensation scheme quantified in terms of a geometrical measure of error. This section now extends this by exploring its effect on the more practically important figures of merit of the antenna's performance. The return loss, S_{11} , and the far field radiation pattern are presented for bending along both the width (H-plane bending), and the length (E-plane bending) of the antenna. Throughout, results are compared to

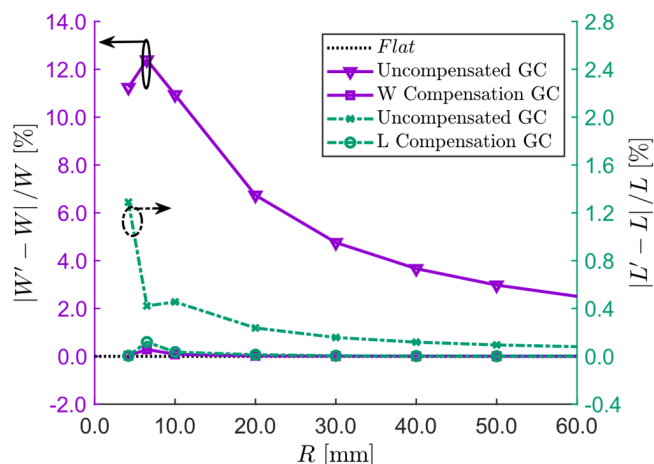


Fig. 9. Relative distortion error along the width and length of antenna to that of the flat antenna for uncompensated and compensated GC generated antennas.

both the *flat* antenna and an *ideal cylindrical* version of the antenna. The geometry of the latter is generated directly in cylindrical coordinates and as such may be regarded as a perfect model without any CAD artefacts for a given sampling resolution and is hence used as the benchmark when comparing against GC generated versions. We show both the results for the GC geometry antenna with and without the compensation applied. Generally, the success of the compensation scheme can be gauged by how close the compensated GC results agree with the *ideal cylindrical* results in Figs 10-13.

The padding value Δ in the GC method is fixed to 6 mm. The WL compensation method uses order (3,3) polynomial surface fitting and iterates until the agreement between the flat and deformed patch width and length agree to a relative tolerance of 0.03%. Fig. 10 compares the return loss, S_{11} , for H-plane bending obtained with the reference antenna geometry and with the uncompensated and compensated GC method along with the flat antenna case for comparison. Two bending radii, $R=6.5$ mm, Fig. 10a) and $R=10$ mm, Fig. 10b) are shown.

First it is seen that the overall impact of H-plane bending on the antenna's resonant frequency is not significant which agrees with published results [13-15]. Second, use of the WL compensated GC geometry predicts a return loss that is in much closer agreement with the reference result than does use of the uncompensated GC geometry.

Fig. 11 repeats analyses the case of E-plane bending. Now the shift of the reference antenna frequency to higher frequencies is more significant compared to the case of H-plane bending as already reported in [13-15]. It is seen that the effect of the uncompensated GC geometry actually leads to a reduction in resonant frequency, i.e. the wrong physical behavior, but again the compensation method has essentially removed this error, yielding excellent agreement with the reference case results. In fact, with the smaller bending radii the relative error in resonant frequency is 0.552% with no discernable error in bandwidth and with the larger bending radii the relative difference in the resonant frequency is 0.0552% and 2.2% in the bandwidth. Finally, it is noted that in both H- and E-plane bending cases the bandwidth is preserved which is in agreement with other published results for cylindrically bent antennas [13-15].

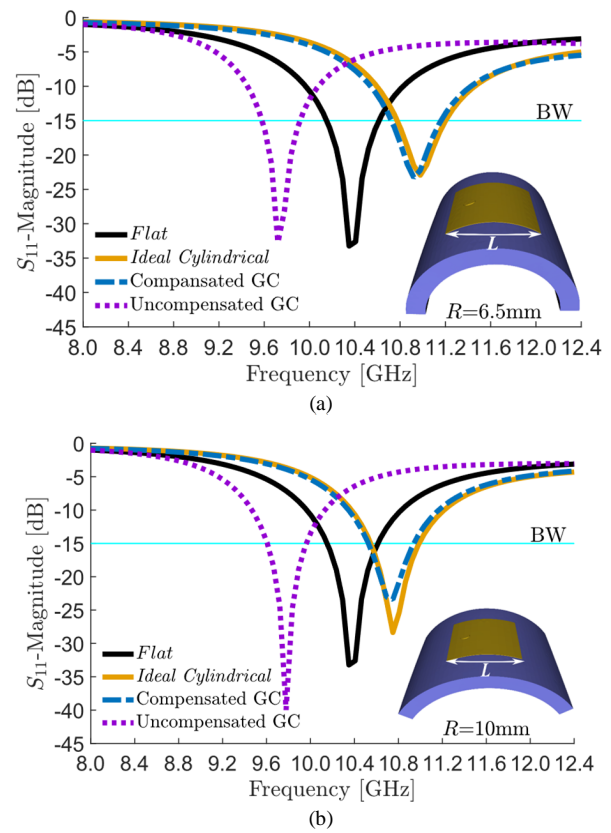
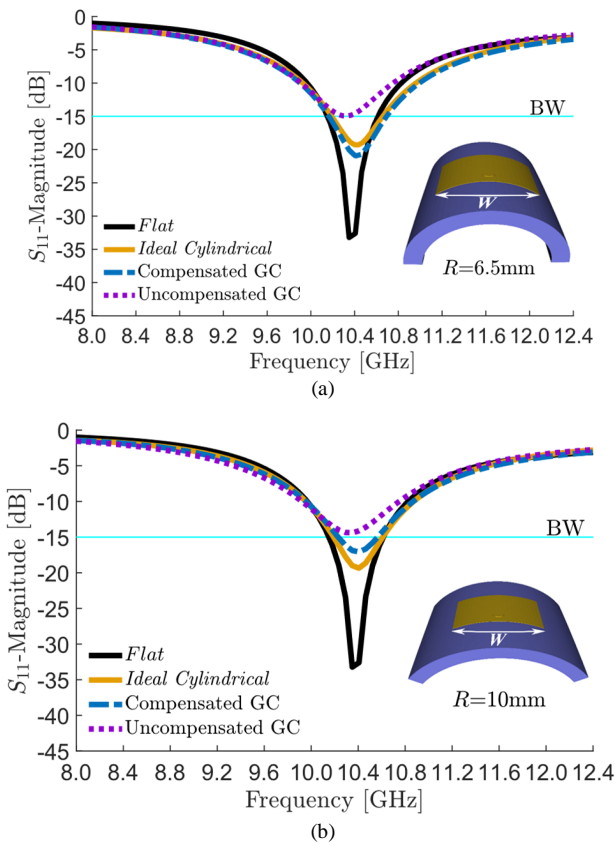


Fig. 10. H-plane Bending: Comparison of S_{11} parameter for the flat antenna and antenna bent in the H-plane using the reference antenna and uncompensated and compensated GC methods for a bending radius of a) $R = 6.5$ mm and b) $R = 10$ mm.

Fig. 11. E-plane bending: Comparison of S_{11} parameter for the flat antenna and antenna bent in the E-plane using the reference antenna and uncompensated and compensated GC methods for a bending radius of a) $R = 6.5$ mm and b) $R = 10$ mm.

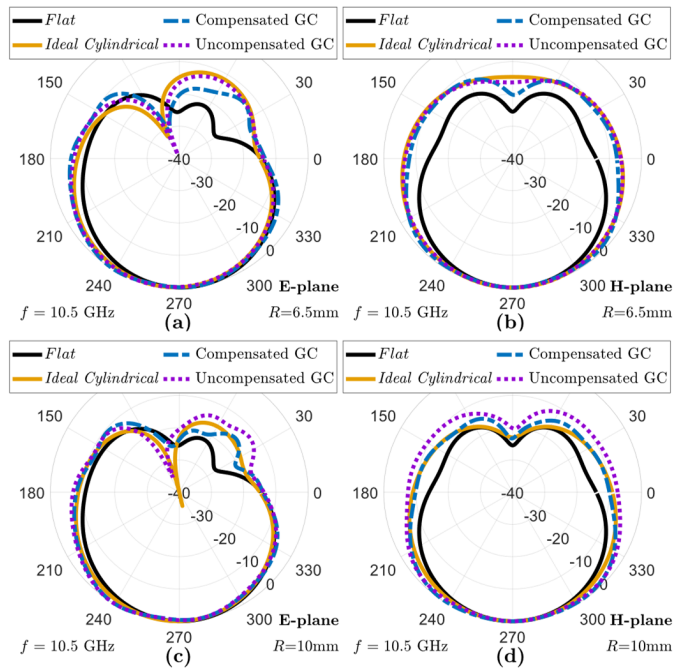


Fig. 12. Normalized far field radiation patterns of antenna bend in the H-plane: (a) E- and (b) H-plane radiation pattern for bending radius of 6.5 mm, and (c) E- and (d) H-plane radiation pattern for bending radius of 10 mm. Results are presented for the flat, ideal cylindrical, uncompensated and compensated GC antennas.

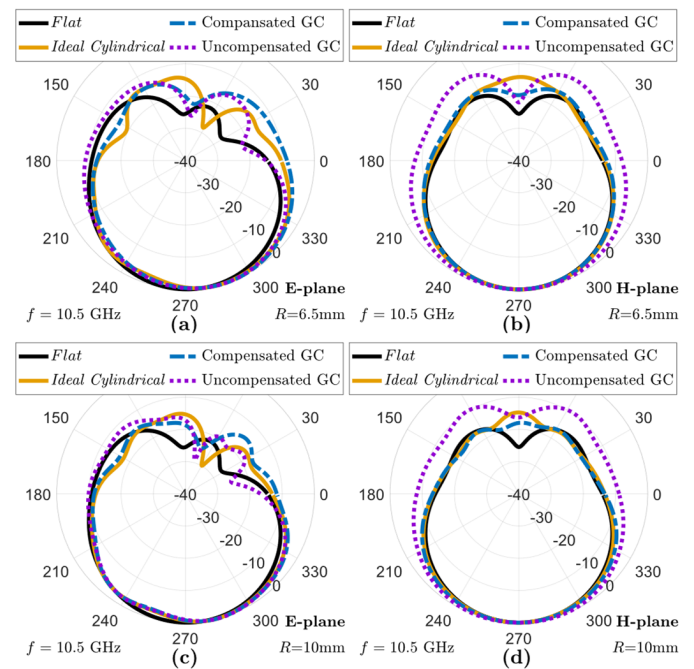


Fig. 13. Normalized far field radiation patterns of antenna bend in the E-plane: (a) E- and (b) H-plane radiation patterns for bending radius of 6.5 mm, and (c) E- and (d) H-plane radiation pattern for bending radius of 10 mm. Results are presented for the flat, ideal cylindrical, uncompensated and compensated GC antennas.

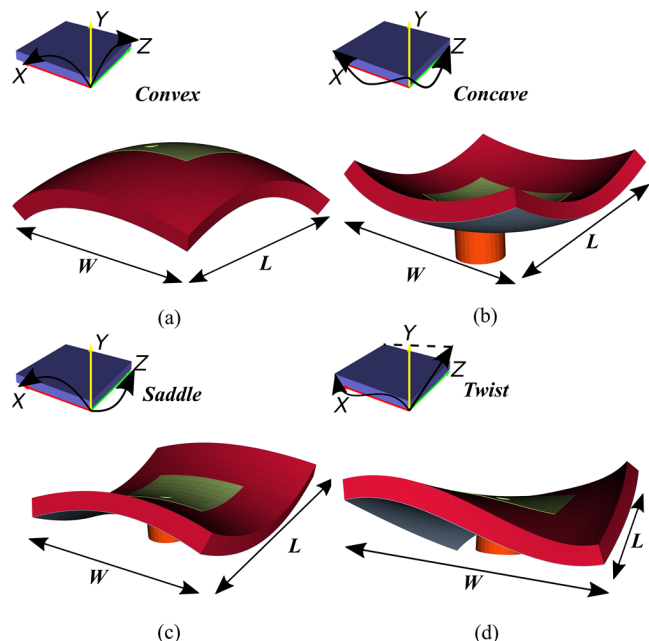


Fig. 14. Arbitrary antenna deformations showing a) convex, b) concave, c) saddle bending and d) antenna under twisting deformation.

Figs. 12 and Figs. 13 complete this validation assessment by presenting the far field radiation patterns for all cases considered in Figs. 10 and 11. The main beam characteristics of the antenna are not significantly affected by bending in either the E or H-planes, but there are some discrepancies in the minor sidelobes.

VI. EM PERFORMANCE OF ARBITRARY DEFORMED ANTENNAS

As stated in the introduction, the driver for this work is not to re-investigate the particular case of cylindrical patch antenna deformations, rather to be able to study the impact of more general shape deformations. However, to reiterate, methodically generating robust geometries has been a significant hurdle to achieving this goal and now that the previous section has successfully validated the use of the WL compensated GC method for this purpose, the remaining space in this paper is dedicated to illustrating its use for the greater challenge. Several canonical antenna deformations that cannot be generated using CSG approaches are considered. These cases are illustrated in Fig. 14 and are labelled as twisted, convex, concave and saddle deformations.

Results using uncompensated GC geometries will still be shown here to emphasize the importance of compensation of the GC distortion errors when assessing the EM performance of such antennas.

For all examples shown, the flat cage is defined using $N=10$ cage segments along both its width and its length and the padding, Δ , is fixed at 3 mm. The reader is reminded that a key attraction of the GC method is that the desired deformations are then simply produced by relocating a few vertices of the flat cage. Here the convex, concave and saddle examples are all produced using different parts of a double curved polygonal deformed cage that is separable; for all three cases the part - cylindrical cage with bending radius of $R = 20$ mm used as in

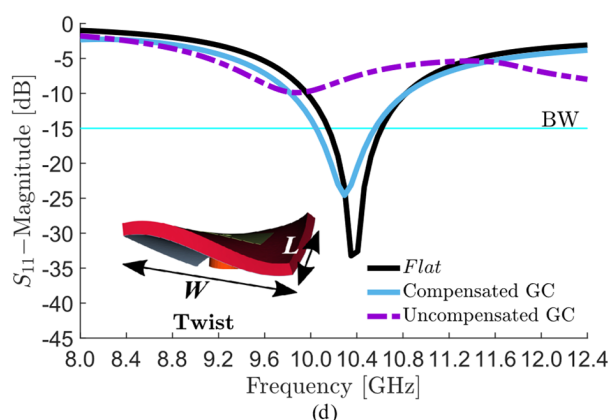
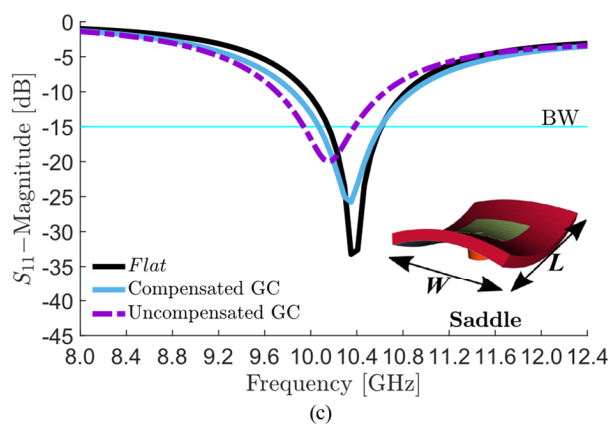
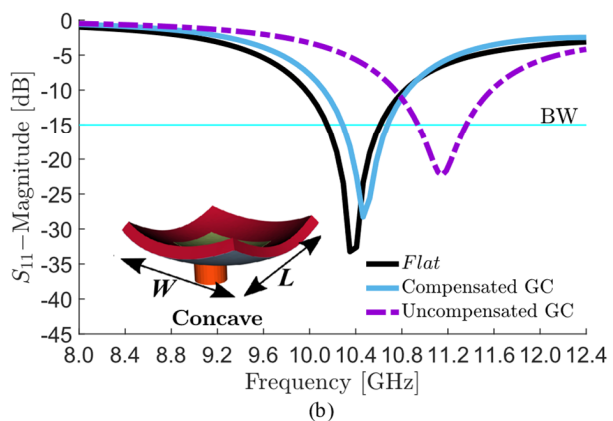
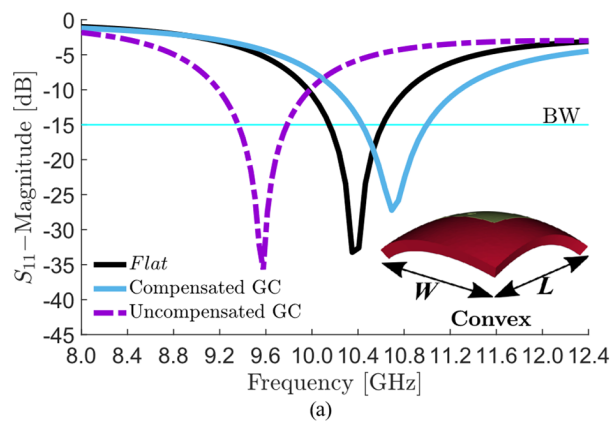


Fig. 15. Return loss S_{11} of the a) convex, b) concave, c) saddle and d) twisted antennas obtained using uncompensated and compensated GC method in comparison with the flat case.

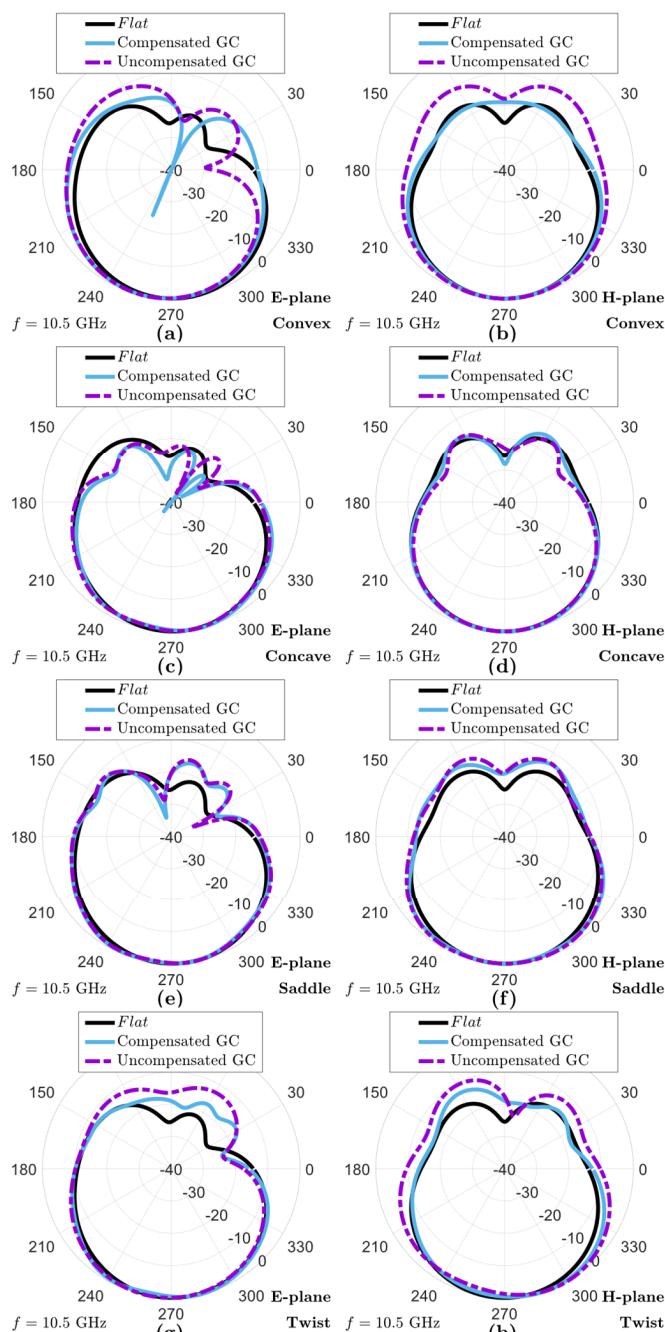


Fig. 16. Normalized far-field pattern in the E- and H-plane of antenna for: (a-b) convex bending, (c-d) concave bending, (e-f) saddle bending, and (g-h) twisting.

Fig. 2 and is further deformed by a half a period of sinusoidal variation of amplitude 10 mm along its length. The twisted case is obtained by applying a simple twisting function of 0.01 radians per-meter to the cuboidal undeformed cage along the length of antenna and sinusoidal deformation of amplitude 10 mm along the width of antenna.

The resulting antenna geometries are presented in Figs. 14 and it is noted here that the GC method is not applied to the coaxial feed.

The electromagnetic performance, in terms of return loss S_{11} and radiation patterns, of the convex, concave, saddle and twisted antennas generated using the uncompensated and compensated GC method are shown in Figs.15 and 16. These

results are compared with the flat case to show the impact of the deformation.

In all cases, the uncompensated GC method produces antenna geometries that significantly underestimate, or overestimate resonant frequency compared to the GC compensation method. We note that all deformations are similar in size but different in their nature. Space precludes an exhaustive discussion of these results here, but it is clear that the size of the resonant frequency shifts are similar in all cases. In fact, comparing convex and concave deformations we can conclude that convex deformation is more detrimental to antenna performance as it leads to a larger frequency shift.

It is acknowledged here that the compensation scheme developed above is only addressing the average distorting effect of the GC method and naturally more work could be undertaken to further tune it for the arbitrarily deformed antenna case. Space precludes expanding on this further here.

VII. CONCLUSION

Modern applications in wearable and foldable electronics are creating increased interest in the performance of antennas subject to in-situ deformations. Unlike traditional conformal antennas whose geometry remains fixed in service, textile antennas must successfully operate whilst suffering a wide range of deformations. This poses new challenges for the antenna designer trying to ensure robust performance. Even systematically defining the, in principle, continuous problem space of the deformations is difficult and from this identifying a finite set of suitable candidates for a testing programme will require a clear understanding of the impact of many possible deformations. It is imperative that complete and systematic studies are undertaken to inform future designs and this paper has addressed a notable hurdle preventing this activity, namely the generation of *robust* and highly variable antenna geometries from a flat prototype.

The GC method provides an approach to holistically deform structures such as patch antennas without introducing the disruptive CAD artefacts that can either block or seriously undermine EM characterization. The method is ideally adapted to a simple *drag and drop* user interface and yields geometries that provide certain guarantees of physical reality in the deformations, albeit not for all the subtleties of woven materials.

This paper has shown that naïve use of the GC method introduces a systematic distortion expressed as an undesirable area scaling. However, this has successfully been compensated for using a straightforward pre-scaling approach, which although not completely general, works well for the widely used class of patch antennas considered here. Furthermore, with the compensation in place a good degree of insensitivity to method parameters such as the padding and complexity of the cage used has been shown which is important for undertaking broad range design studies.

After calibration against a known canonical case whose geometry can be exactly generated, final GC generated antenna performance in terms of return loss and radiation patterns have been examined and shown good agreement with published

1 results. Finally, the scope to address the grander challenge of
 2 undertaking a systematic design sweep over the problem space
 3 of possible doubly curved deformations has been demonstrated
 4 and results from this activity will be the subject of a future
 5 contribution.

REFERENCES

- 6
- 7
- 8
- 9
- 10
- 11
- 12
- 13
- 14
- 15
- 16
- 17
- 18
- 19
- 20
- 21
- 22
- 23
- 24
- 25
- 26
- 27
- 28
- 29
- 30
- 31
- 32
- 33
- 34
- 35
- 36
- 37
- 38
- 39
- 40
- 41
- 42
- 43
- 44
- 45
- 46
- 47
- 48
- 49
- 50
- 51
- 52
- 53
- 54
- 55
- 56
- 57
- 58
- 59
- 60
- [1] R. Salvado, C. Loss, R. Gonçalves, and P. Pinho, "Textile Materials for the Design of Wearable Antennas: A Survey," (in English), *Sensors*, vol. 12, no. 11, pp. 15841-15857, 2012.
- [2] L. M. Castano and A. B. Flatau, "Smart fabric sensors and e-textile technologies: a review," *Smart Materials and Structures*, vol. 23, no. 5, p. 053001, 2014/04/01 2014, doi: 10.1088/0964-1726/23/5/053001.
- [3] S. Rao *et al.*, "Miniature implantable and wearable on-body antennas: towards the new era of wireless body-centric systems [antenna applications corner]," *IEEE Antennas and Propagation Magazine*, vol. 56, no. 1, pp. 271-291, 2014.1109/MAP.2014.6821799.
- [4] J. Monica and P. Jothilakshmi, "Gain enhanced conformal patch antenna with defected ground for aircraft applications," *IET Communications*, vol. 14, no. 2, pp. 290-299, 2020, doi: 10.1049/iet-com.2018.6042.
- [5] S. F. Jilani, M. O. Munoz, Q. H. Abbasi, and A. Alomainy, "Millimeter-Wave Liquid Crystal Polymer Based Conformal Antenna Array for 5G Applications," (in en), *IEEE Antennas and Wireless Propagation Letters*, vol. 18, no. 1, pp. 84-88, 2019/01/11 2019, doi: 10.1109/LAWP.2018.2881303.
- [6] I. Locher, M. Klemm, T. Kirstein, and G. Troster, "Design and Characterization of Purely Textile Patch Antennas," *IEEE Transactions on Advanced Packaging*, vol. 29, no. 4, pp. 777-788, 2006, doi: 10.1109/tadvp.2006.884780.
- [7] C. Hertleer, A. Tronquo, H. Rogier, L. Vallozzi, and L. Van Langenhove, "Aperture-Coupled Patch Antenna for Integration Into Wearable Textile Systems," *IEEE Antennas and Wireless Propagation Letters*, vol. 6, pp. 392-395, 2007, doi: 10.1109/lawp.2007.903498.
- [8] S. Zhu and R. Langley, "Dual-Band Wearable Textile Antenna on an EBG Substrate," *IEEE Transactions on Antennas and Propagation*, vol. 57, no. 4, pp. 926-935, 2009, doi: 10.1109/TAP.2009.2014527.
- [9] Y. Bayram *et al.*, "E-Textile Conductors and Polymer Composites for Conformal Lightweight Antennas," *IEEE Transactions on Antennas and Propagation*, vol. 58, no. 8, pp. 2732-2736, 2010, doi: 10.1109/TAP.2010.2050439.
- [10] Y. Zhou, Y. Bayram, F. Du, L. Dai, and J. L. Volakis, "Polymer-Carbon Nanotube Sheets for Conformal Load Bearing Antennas," *IEEE Transactions on Antennas and Propagation*, vol. 58, no. 7, pp. 2169-2175, 2010, doi: 10.1109/TAP.2010.2048852.
- [11] Z. Wang, L. Zhang, Y. Bayram, and J. L. Volakis, "Embroidered Conductive Fibers on Polymer Composite for Conformal Antennas," *IEEE Transactions on Antennas and Propagation*, vol. 60, no. 9, pp. 4141-4147, 2012, doi: 10.1109/TAP.2012.2207055.
- [12] Z. Wang, L. Z. Lee, D. Psychoudakis, and J. L. Volakis, "Embroidered Multiband Body-Worn Antenna for GSM/PCS/WLAN Communications," *IEEE Transactions on Antennas and Propagation*, vol. 62, no. 6, pp. 3321-3329, 2014, doi: 10.1109/TAP.2014.2314311.
- [13] F. Boeykens, H. Rogier, and L. Vallozzi, "An Efficient Technique Based on Polynomial Chaos to Model the Uncertainty in the Resonance Frequency of Textile Antennas Due to Bending," *IEEE Transactions on Antennas and Propagation*, vol. 62, no. 3, pp. 1253-1260, 2014, doi: 10.1109/tap.2013.2294021.
- [14] D. Ferreira, P. Pires, R. Rodrigues, and R. F. S. Caldeirinha, "Wearable Textile Antennas: Examining the effect of bending on their performance," *IEEE Antennas and Propagation Magazine*, vol. 59, no. 3, pp. 54-59, 2017, doi: 10.1109/map.2017.2686093.
- [15] L. Song and Y. Rahmat-Samii, "A Systematic Investigation of Rectangular Patch Antenna Bending Effects for Wearable Applications," *IEEE Transactions on Antennas and Propagation*, vol. 66, no. 5, pp. 2219-2228, 2018, doi: 10.1109/tap.2018.2809469.
- [16] S.-E. Adami *et al.*, "A Flexible 2.45-GHz Power Harvesting Wristband With Net System Output From -24.3 dBm of RF Power," *IEEE Transactions on Microwave Theory and Techniques*, vol. 66, no. 1, pp. 380-395, 2018, doi: 10.1109/tmtt.2017.2700299.
- [17] J. Zhong, A. Kiourtii, T. Sebastian, Y. Bayram, and J. L. Volakis, "Conformal Load-Bearing Spiral Antenna on Conductive Textile Threads," *IEEE Antennas and Wireless Propagation Letters*, vol. 16, pp. 230-233, 2017, doi: 10.1109/LAWP.2016.2570807.
- [18] M. S. Floater, G. Kós, and M. Reimers, "Mean value coordinates in 3D," *Computer Aided Geometric Design*, vol. 22, no. 7, pp. 623-631, 2005, doi: 10.1016/j.cagd.2005.06.004.
- [19] P. Joshi, M. Meyer, T. DeRose, B. Green, and T. Sanocki, "Harmonic coordinates for character articulation," *ACM Transactions on Graphics*, vol. 26, no. 99, 2007, doi: 10.1145/1276377.1276466.
- [20] Y. Lipman, D. Levin, and D. Cohen-Or, "Green Coordinates," *ACM Trans. Graph.*, vol. 27, no. 3, pp. 1-10, 2008, doi: 10.1145/1360612.1360677.
- [21] Y. Lipman and D. Levin, "Derivation and Analysis of Green Coordinates," *Computational Methods and Function Theory*, journal article vol. 10, no. 1, pp. 167-188, June 01 2010, doi: 10.1007/bf03321761.
- [22] E. Altinozen, I. Harrison, A. Vukovic, and P. D. Sewell, "Green Coordinates for Generation of Conformal Antenna Geometries," in *2020 14th European Conference on Antennas and Propagation (EuCAP)*, 15-20 March 2020 2020, pp. 1-5, doi: 10.23919/EuCAP48036.2020.9135814. [Online]. Available: <https://ieeexplore.ieee.org/document/9135814/>
- [23] A. Vukovic, S. Zongyuan, P. Sewell, L. A. Aziz, and T. M. Benson, "Geometric challenges of modelling textile antennas," in *2017 European Modelling Symposium (EMS)*, 2017: IEEE, pp. 34-37.
- [24] P. Sewell, T. M. Benson, C. Christopoulos, D. W. P. Thomas, A. Vukovic, and J. G. Wykes, "Transmission-line modeling (TLM) based upon unstructured tetrahedral meshes," *IEEE Transactions on Microwave Theory and Techniques*, vol. 53, no. 6, pp. 1919-1928, 2005, doi: 10.1109/TMTT.2005.848078.
- [25] P. D. Sewell, T. M. Benson, C. Christopoulos, D. W. P. Thomas, A. Vukovic, and J. G. Wykes, "Implicit Element Clustering for Tetrahedral Transmission-Line Modeling (TLM)," *IEEE Transactions on Microwave Theory and Techniques*, vol. 57, no. 8, pp. 2005-2014, 2009, doi: 10.1109/TMTT.2009.2025451.
- [26] GGIEMR. "George Green Institute for Electromagnetics Research." <https://www.nottingham.ac.uk/research/groups/ggiemr/our-research/large-scale-electromagnetic-modelling/utlm-unstructured-transmission-line-modelling.aspx> (accessed 2021).
- [27] S. W. Cheng, T. K. Dey, and J. Shewchuk, *Delaunay Mesh Generation*. CRC Press, 2013.
- [28] C. Jones, P. Sewell, T. M. Benson, A. Vukovic, X. Meng, and H. Bucklow, "Advanced computational electromagnetics at BAE systems," 2016.
- [29] X. Meng, A. Vukovic, T. M. Benson, and P. Sewell, "Extended Capability Models for Carbon Fiber Composite (CFC) Panels in the Unstructured Transmission Line Modeling (UTLM) Method," *IEEE Transactions on Electromagnetic Compatibility*, vol. 58, no. 3, pp. 811-819, 2016, doi: 10.1109/temc.2016.2531791.
- [30] X. Meng, P. Sewell, N. H. Rahman, A. Vukovic, and T. M. Benson, "Experimental benchmarking of unstructured transmission line modelling (UTLM) method in modelling twisted wires," *ACES Express Journal*, vol. 1, no. 3, 2016.
- [31] P. Sewell, A. Vukovic, T. M. Benson, and X. Meng, "Extracting modal field profiles from 3D unstructured transmission line modelling meshes for use as sources and observers," *IET Science, Measurement & Technology*, vol. 11, no. 6, pp. 780-785, 2017, doi: 10.1049/iet-smt.2016.0357.
- [32] A. Vukovic, P. Sewell, T. M. Benson, C. Earl, and C. Jones, "Modelling of structural joints for lightning direct effect studies," in *Tenth International Conference on Computational Electromagnetics (CEM 2019)*, 19-20 June 2019 2019, pp. 1-5, doi: 10.1049/cp.2019.0125.
- [33] A. Vukovic, P. Sewell, and T. M. Benson, "Holistic Appraisal of Modeling Installed Antennas for Aerospace Applications," *IEEE Transactions on Antennas and Propagation*, vol. 67, no. 3, pp. 1396-1409, 2019, doi: 10.1109/tap.2018.2884769.
- [34] A. Vukovic, P. Sewell, and T. M. Benson, "Impact of In Situ Radome Lightning Diverter Strips on Antenna Performance," *IEEE Transactions on Antennas and Propagation*, vol. 68, no. 11, pp. 7287-7296, 2020, doi: 10.1109/TAP.2020.2998169.
- [35] C. Christopoulos, *The transmission-line modeling method: TLM*. IEEE press, 1995.
- [36] P. Russer, in *The transmission line matrix method, in applied computational electromagnetics*: Springer-Verlag, 2000.
- [37] X. Meng, P. Sewell, A. Vukovic, Z. Zhang, and T. Benson, "Experimental benchmarking of unstructured transmission line

1 modelling (UTLM) method for simulations of explicitly meshed
 2 wiring," in *2015 Computational Electromagnetics International*
 3 *Workshop (CEM)*, 1-4 July 2015, pp. 1-2, doi:
 4 10.1109/CEM.2015.7237433.



5 **Ekrem Altinozen** received the B.S.
 6 degree in electrical and electronic
 7 engineering from Eskisehir Osmangazi
 8 University, Eskisehir, Turkey, in 2015,
 9 and the M.S. degree (with first-class
 10 honors) from University of Nottingham,
 11 Nottingham, U.K. in 2018, where he is
 12 currently pursuing the Ph.D degree. His current research
 13 interests conformal, wearable and foldable antennas and
 14 interconnects for personal and industrial applications.
 15



16 **Ian Harrison** was born in the north-west
 17 of England in 1961. He received a BSc
 18 degree in Physics (with first class) from the
 19 University of Nottingham and a PhD from
 20 the University of Manchester, Manchester
 21 UK in 1982 and 1986 respectively. In 1987
 22 he joined the School of Electrical and Electronic Engineering
 23 and retired in 2020 has a full Professor.
 24



25 **Ana Vukovic** (M'97) was born in Nis,
 26 Serbia, in 1968. She received the Diploma
 27 of Engineering degree in electronics and
 28 telecommunications from the University
 29 of Nis, Nis, Yugoslavia, in 1992, and the
 30 Ph.D. degree from the University of
 31 Nottingham, Nottingham, U.K., in 2000.
 32 From 1992 to 2001, she was a Research Associate with the
 33 University of Nottingham. In 2001, she joined the School of
 34 Electrical and Electronic Engineering, University of
 35 Nottingham, as a Lecturer. Her research interests are
 36 electromagnetics with a particular emphasis on applications in
 37 optoelectronics, microwaves, and EMC.
 38



39 **Phillip Sewell** (M'89-SM'04) was born in
 40 London, U.K., in 1965. He received the
 41 B.Sc. degree in electrical and electronic
 42 engineering (with first-class honors) and
 43 Ph.D. degree from the University of Bath,
 44 Bath, U.K., in 1988 and 1991, respectively.
 45 From 1991 to 1993, he was a Post-Doctoral
 46 Fellow with the University of Ancona,
 47 Ancona, Italy. In 1993, he became a Lecturer with the School
 48 of Electrical and Electronic Engineering, University of
 49 Nottingham, Nottingham, U.K. In 2001 and 2005, he became a
 50 Reader and Professor of electromagnetics at the University of
 51 Nottingham. His research interests involve analytical and
 52 numerical modeling of electromagnetic problems with
 53 application to opto-electronics, microwaves and aerospace
 54 applications.
 55
 56
 57
 58
 59
 60